J. Chem. Sci. Vol. 128, No. 7, July 2016, pp. 1081–1093.
DOI 10.1007/s12039-016-1111-3

Synthesis, crystal structure, thermal and theoretical studies of bis(*N*-ethyl-*N*-phenyldithiocarbamato) Ni(II) and (*N*-ethyl-*N*-phenyldithiocarbamato) (isothiocyanato) (triphenylphosphine) Ni(II)

DAMIAN C ONWUDIWE[a,b,*], MWADHAM M KABANDA[a,b], ENO E EBENSO[a,b] and ERIC HOSTEN[c]

[a]Material Science Innovation and Modelling (MaSIM) Research Focus Area, Faculty of Agriculture, Science and Technology, North-West University (Mafikeng Campus), Private Bag X2046, Mmabatho, South Africa
[b]Department of Chemistry, School of Mathematical and Physical Sciences, Faculty of Agriculture, Science and Technology, North-West University (Mafikeng Campus), Private Bag X2046, Mmabatho 2735, South Africa
[c]Department of Chemistry, Nelson Mandela Metropolitan University, P.O Box 77000, Port Elizabeth 6031, South Africa
e-mail: Damian.Onwudiwe@nwu.ac.za

MS received 25 January 2016; revised 27 April 2016; accepted 28 April 2016

Abstract. Homoleptic and heteroleptic Ni(II) complexes represented as $\mathbf{NiL^1_2}$ and $\mathbf{NiL^1L^2L^3}$ (where, L^1 = *N*-ethyl-*N*-phenyldithiocarbamato anion, L^2 = isothiocyanato anion, and L^3 = triphenylphosphine) were synthesized. The complexes have been characterized by elemental, IR, NMR, and single-crystal X-ray analysis. The thermal decomposition behaviour of the complexes were studied using thermogravimetric analysis (TGA). The optimized geometry and the electronic analysis of the type of bonding within the complex structures were performed using methods based on the density functional theory and atom in molecule (AIM) analysis method. X-ray structural analysis of both complexes confirms distorted square planar geometry about the Ni atom. The TGA indicates that the complexes belong to the class of volatile dithiocarbamates which yield the corresponding metal sulphide without any intermediate products. Structural parameters from crystallographic and DFT studies have been compared and found to correlate with each other. The small discrepancies in geometric parameters are attributable to H-bonding and packing interactions within the lattice which are not modelled during computational study. AIM analysis suggests that in $\mathbf{NiL^1L^2L^3}$, the Ni$\cdots$L interactions are more covalent in nature whereas in $\mathbf{NiL^1_2}$ complex, they are more ionic in character.

Keywords. Nickel(II); dithiocarbamate; thermal studies; crystal structure; DFT.

1. Introduction

Dithiocarbamate ligand has been used to prepare different transition metal complexes with various compositions, geometries, and properties.[1] It exhibits remarkable diversity in the bonding/coordination possibilities with nickel.[2] The coordination chemistry of nickel(II) encompasses a variety of geometry and coordination numbers.[3] Octahedral nickel(II) dithiocarbamate complexes involving bidentate and tetradentate nitrogen-donor ligands have been reported.[4] Bis(dithiocabamato) nickel(II) complexes in four coordinate environment are planar, diamagnetic, and invariably show asymmetry in Ni-S bonds; and this has been ascribed to the variations in the nature of the substituents.[5]

As common among the group 10 dithiolate complexes which contain the planer MS_4 chromophores, Ni(II) dithiocarbamates show interesting reactions with Lewis bases,[6] Ni(II) is a border line acceptor, unlike the other group 10 elements (Pt and Pd). Due to symbiotically induced softness, it prefers to react with soft Lewis bases such as phosphines rather than hard nitrogenous bases such as ammonia and pyridine.[7] The adducts of Ni(II) dithiocarbamate obtained from the Lewis bases have been in the limelight on account of their structural novelty and interesting biological properties. The complexes displayed interesting electrochemical properties and higher antimicrobial activity compared with the commercially available antibiotics, and have found application in various areas such as catalysts in cross-coupling reactions and medicine.[8–11] They are also used as effective light stabilizers for olefins,[12] and recently as precursors for the preparation of nanoparticles.[13] Ni(II) complexes do not stabilize their geometries effectively under various chemical environments. The study of

*For correspondence

different planar Ni(II) complexes are important, since planar Ni(II) complexes rather than their platinum analogues are preferable for specialised applications under biochemical environments due to reduced toxicity. Different Ni(II) dithiocarbamate with planar NiS_2P_2, NiS_2PN, and NiS_2PC chromophores have been synthesized.[14–17] The steric and electronic effects of the substituents on the complexes have also been studied.[18,19]

Furthermore, a series of neutral nickel(II) complexes have been used to study the interaction of complexes with calf thymus DNA, bovine serum albumin (BSA) and human serum albumin (HSA).[20] Nickel(II) complexes containing ONS donor ligands have been applied as catalyst towards C-C cross-coupling reactions.[21] Different nickel complexes with nuclease activity have been reported in literature.[22–24] In order to study the structure and properties of the nickel(II) dithiocarbamate complex with homoleptic and heteroleptic system, we report here the synthesis, structural characterization, thermal and theoretical studies of Ni(II) dithiocarbamate complex and its adduct with triphenylphosphine and thiocyanate.

2. Experimental

2.1 *Materials and methods*

All chemicals and solvents used in this work were obtained from commercial sources. They are of analytical grade and were used as received. The complexes were prepared by a slightly modified procedure described previously.[25] Elemental analysis was performed in an Elementar, Vario EL Cube, set up for CHNS analysis. Infrared spectra were recorded on a Bruker alpha-P FT-IR spectrometer in the frequency range 4000–500 cm^{-1}. ^1H and ^{13}C NMR spectra were recorded on a 600 MHz Bruker Avance III NMR spectrometers using $CDCl_3$ as solvent and tetramethylsilane (TMS) as internal standard. Simultaneous thermogravimetric (TG) and differential scanning calorimetry (DSC) analysis was performed on SDTQ 600 thermal instrument under nitrogen atmosphere with 10°C as heating rate.

2.2 *Synthesis of complexes*

2.2a *Bis(N-ethyl-N-phenyldithiocarbamato)nickel(II),* $\boldsymbol{NiL_2^1}$: *N*-ethyl aniline (3.22 mL, 0.025 mol) was reacted with a solution of CS_2 (1.5 mL, 0.025 mol) in ethanol (25 mL) under ice cold condition. The reaction mixture was left to stand for 10 min. To this mixture, a solution of $NiNO_3{\cdot}6H_2O$ (3.63 g, 0.0125 mmol) in distilled water (25 mL) was added slowly and stirred vigorously. A deep green precipitate was formed, and the reaction was allowed to proceed for 1 h. The product was then filtered off, washed with warm ethanol-water mixture (1:3), and dried in vacuo. Single crystals suitable for X-ray analysis were obtained from chloroform/toluene. Yield: 76%; M.p: 195°C; Anal. Calc. (%) for $C_{18}H_{20}N_2S_4Ni$: C: 47.90; H: 4.47; N: 6.21; S: 28.42. Found (%): C: 48.12; H: 4.42; N: 6.40; S: 28.37.

2.2b *(N-ethyl-N-phenyldithiocarbamato)(isothiocyanato)(triphenylphosphine) Nickel(II),* $\boldsymbol{NiL^1L^2L^3}$: A mixture of bis(*N*-ethyl-*N*-phenyldithiocarbamate) Ni(II) (0.11 g, 0.25 mmol), PPh_3 (0.13 g, 0.5 mmol), $NiCl_2{\cdot}6H_2O$ (0.060 g, 0.25 mmol), and NH_4SCN (0.04 g, 0.5 mmol) was refluxed for 3h in an acetonitrile-methanol mixture (2:1, 30 mL). The dark purple-red solution obtained was allowed to cool down, filtered and left to evaporate. After 4 days, crystals were obtained which were again recrystallized using the same solvent system to afford single crystals suitable for X-ray analysis. Yield: 71%; M.p.: 173°C; Anal. Calc. (%) for $C_{28}H_{25}N_2NiPS_3$: C: 58.45; H: 4.38; N: 4.87; S: 16.72 Found (%): C: 58.41; H: 4.18; N: 5.03, S: 16.70.

The schematic routes to the synthesis of complexes $\mathbf{NiL_2^1}$ and $\mathbf{NiL^1L^2L^3}$ are presented in scheme 1.

2.3 *X-ray crystallography*

X-ray diffraction studies of $\mathbf{NiL_2^1}$ and $\mathbf{NiL^1L^2L^3}$ were performed at 200 K using a Bruker Kappa Apex II diffractometer with graphite monochromated MoKα radiation ($\lambda = 0.71073$ Å). APEXII was used for data collection and SAINT for cell refinement and data reduction.[26] The structures were solved by direct methods using SHELXS-2014, and refined by least-squares procedures using SHELXL-2014[27] with SHELXLE[28] as a graphical interface. All non-hydrogen atoms were refined anisotropically, and the hydrogen atoms were calculated in idealized geometrical positions. The H atoms of the ethyl groups were allowed to rotate with a fixed angle around the C–C bond to best fit the experimental electron density (HFIX 137 in the SHELX program suite[27]), with Uiso(H) set to 1.5Ueq(C). Data were corrected for absorption effects by the numerical methods using SADABS.[26]

2.4 *Computational Details*

The geometry optimisation was performed using the density functional theory with the Becke three parameter

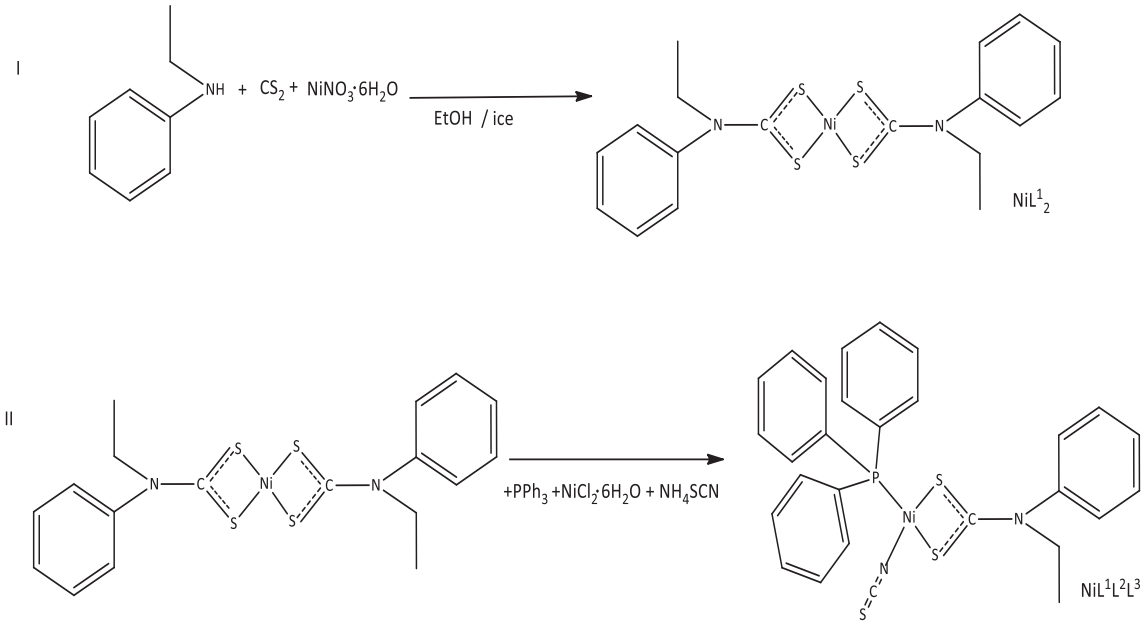

Scheme 1. The schematic route to the synthesis of complexes (I) NiL^1_2 and (II) $NiL^1L^2L^3$.

lee Yang Parr functional (B3LYP); the C, N, P, S and H atoms were optimised using the 6-31+G(d,p) basis set while the Ni atom was optimised using the LANL2DZ functional. Frequency calculations were performed, at the same level of calculations as the geometry optimisation, on fully optimised conformers, to determine the nature of the stationary points.

All calculations were performed using the Gaussian09 program.[29] The schematic representations were drawn using the Chem Office package in the UltraChem 2010 version and conformers were drawn using GaussView5 program.

The Quantum Mechanics Atoms in Molecule (QMAIM) was performed using the AIMAll program.[30]

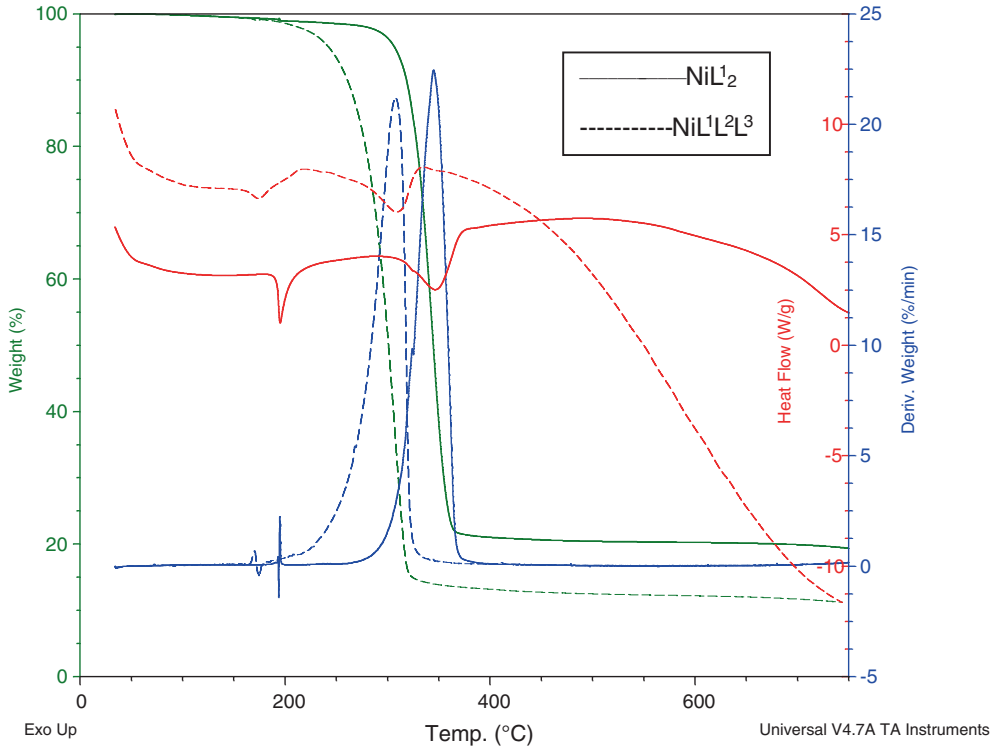

Figure 1. TG/DTG and DSC curves of the compounds NiL^1_2 and $NiL^1L^2L^3$ obtained in nitrogen atmosphere (75 mL/min), heating rate 10°C/min.

The number of critical points (CP) found for all of the analysed systems are in agreement with the Poincare–Hopf rule. The following parameters of the bond critical point (BCP) were analysed: the electron density (ρ) and its Laplacian ($\nabla^2\rho$), the total energy density of electrons (H), and its two components, the Lagrangian kinetic electron density (G) and the potential electron density (V). The total energy density, H, was estimated as the sum of the kinetic electron density (G) and potential energy density (V):

$$H_{BCP} = G_{BCP} + V_{BCP} \quad (1)$$

3. Results and Discussion

3.1 *IR spectral studies*

The two complexes showed distinct vibrational band around 1000 cm^{-1} which is associated with the symmetric bidentate $\nu(CS_2)$ vibration of the dithiocarbamate ligand. The characteristic band of the thioureide vibration associated with the ν(C==N) appeared at 1492 cm^{-1} in $\mathbf{NiL^1_2}$, and 1500 cm^{-1} in $\mathbf{NiL^1L^2L^3}$. The appreciable higher value observed than that in the free ligand (1456 cm^{-1})[31] indicates significant increase in the partial double bond character of C–N bond.[32] An increase in the drift of electron density from the dithiocarbamate towards the metal center is responsible for the increase in the thioureide stretching bands to higher frequencies in $\mathbf{NiL^1L^2L^3}$.[29] The $\nu(C_2–N)$ stretching vibrations were observed at 1283 and 1289 cm^{-1} for $\mathbf{NiL^1_2}$ and $\mathbf{NiL^1L^2L^3}$ respectively. The spectrum of $NiL^1L^2L^3$ showed the band resulting from the N-coordinated thiocyanate at 2078 cm^{-1}.

3.2 *NMR spectral studies*

The ^{1}H-NMR spectrum of complex NiL^1_2 showed that the α-methylene and the methyl group protons appeared at 3.95 and 0.85 ppm respectively. However, in the spectrum of the heteroleptic complex $\mathbf{NiL^1L^2L^3}$, the α-methylene protons appeared as broad doublets with peaks at 3.96 and 3.79 ppm, while the terminal methyl group protons were observed at 1.08 ppm. The broadening of the aliphatic proton signals is ascribed to the fast ligand exchange process observed in [Ni(dtc)(PPh3)X] (X = Cl, Br, I, NCS) complexes,[33,34] and the great deshielding of the α-methylene protons is due to the high electronegativity of the nitrogen atom. The aromatic protons resonate in the region 7.12–7.43 ppm in complex $\mathbf{NiL^1_2}$ and 7.10–7.52 ppm in complex $\mathbf{NiL^1L^2L^3}$. The signals due to the protons of the phosphine group appear between 7.64–7.77 ppm. In the ^{13}C NMR spectra, the signals at 209.6 and 206.2 ppm, with very weak intensity characteristic of quaternary carbon signals, correspond to the NCS_2 function in complexes $\mathbf{NiL^1_2}$ and $\mathbf{NiL^1L^2L^3}$ respectively. The upfield shift of 3.4 ppm observed in complex $\mathbf{NiL^1L^2L^3}$ compared with that of the parent complex NiL^1_2 is due to the presence of the π-accepting phosphine (triphenylphosphine) in $NiL^1L^2L^3$ which increases the mesomeric drift of electron density from the dithiocarbamate moiety toward the metal atom. Consequently, this results in an increase in the $N^{\delta+}$.....$C^{\delta-}$ partial double bond character, and a displacement of the electron density from the nitrogen atom of the dithiocarbamate group.[35] The signals observed in the downfield region, 127.2–139.6 ppm in complex NiL^1_2 and 126.8–134.0 in $\mathbf{NiL^1L^2L^3}$, are due to the aromatic protons. The methylene carbons on the nitrogen atom are greatly deshielded and were observed at 47.9 ppm in both complexes, while the methyl group carbons resonated at 12.51 for complex $\mathbf{NiL^1_2}$ and 12.40 for $\mathbf{NiL^1L^2L^3}$. The thiocyanate (NCS) carbon resonates around 142 ppm.

3.3 *Thermal studies*

The TG-DTG/DSC curves in nitrogen atmosphere are shown in Figure 1 and the data are presented in Table 1. In both complexes, decomposition started at a temperature above 150°C, which indicates the absence of solvent molecules. The decomposition occurs in one single step in the range 268–385°C and 190–339°C for complexes $\mathbf{NiL^1_2}$ and $\mathbf{NiL^1L^2L^3}$ respectively, with the temperature of the maximum rate of decomposition occurring around 344 and 307°C. This indicates that $\mathbf{NiL^1_2}$ has higher thermal stability than $\mathbf{NiL^1L^2L^3}$; and it is ascribed to the replacement of the sulphur atoms in the NiS_4 chromophore of $\mathbf{NiL^1_2}$ by the P and N atoms in $\mathbf{NiL^1L^2L^3}$, thereby resulting in a decrease in the decomposition temperature of the complex.[36] In both complexes, there was no formation of thiocyanate intermediate. The formation of metal thiocyanates as an intermediate product resulting from the decomposition of the organic portion of dithiocarbamate complexes is well established.[37–39] The TGA curves of the two complexes indicates that

Table 1. Result from TG/DTG and DSC curves of complexes NiL12 and NiL1L2L.

Compounds	NiL^1_2	$NiL^1L^2L^3$
Decomposition range (°C)	268–385	190–339
DTG peak, T(°C)	344	307
DSC peak, T(°C)	347	310
Melting point (DTG/°C)	194	170
Melting point (DSC/°C)	195	173
Mass loss (mg)		
Found	2.50	1.02
Calc.	2.47	1.13

they belong to the class of volatile dithiocarbamates which yield the corresponding metal sulphide without any intermediate products.[40] All the ligand components in **NiL^{1}L^{2}L^3** (*i.e.*, L^1, L^2, and L^3) undergo a simultaneous decomposition probably due to close temperatures of desorption from the metal atom. The mass of the residue found at the end of the decomposition of **NiL$_2^1$** and **NiL^{1}L^{2}L^3** were 2.50 and 1.02 mg respectively, and this corresponds to NiS (expected: 2.47 and 1.13 mg respectively).

The DSC curves of both complexes have two endothermic peaks. The first peaks which appeared at 195 and 173°C for **NiL$_2^1$** and **NiL^{1}L^{2}L^3** respectively showed no weight loss in the TG, and it is attributed to the melting of the complexes. The second endothermic peaks appeared at 347 and 310°C and are associated with the decomposition of the complex. The presence of only one peak in this decomposition step indicates the absence of the metal thiocyanates in the TG experiment and the higher values of **NiL$_2^1$** compared to **NiL^{1}L^{2}L^3** supports the high thermal stability of the former.

3.4 *Crystal structure*

Crystals suitable for single crystal X-ray structural analysis were obtained for both complexes using the method of slow evaporation of two-solvent system. The ORTEP diagram of complex **NiL$_2^1$** is given in Figure 2. Details of the crystal data and structure refinement parameters are summarized in Table 2. Selected bond lengths and angles are given in Table 3. The complex crystallizes in the monoclinic *P*21/*n* space group with the unit cell parameters a = 7.4619 (3) Å, b = 7.0012 (3) Å, c = 19.2781 (9) Å, and z = 2. Its structure consists of mononuclear neutral species in which the Ni(II) central atom is surrounded by four sulphur atoms from two bidentate dithiocarbamate ligands in a distorted square planar environment. Each of the dithiocarbamate ligands forms a four-membered chelate rings. The observed distortion of the square planar coordination around nickel is attributed to the small bite angle of the dithiocarbamate ligand [79.66 (1)°]. The four Ni–S bonds give a centrosymmetrical complex. The Ni(1)–S(1) and Ni(1)–S(1a) bond lengths are essentially the same at 2.2106(4) Å, while their *cis* Ni(1)–S(2) and Ni(1)–S(2)a bond lengths are also the same at 2.1917(4) Å. The C–S bond lengths are 1.7115(14) and 1.7187(13) Å, and are shorter than the typical single bond length of 1.82 Å but longer than the C=S double bond distance of 1.67 Å.[41] The intermediate value of the CS indicates the partial double bond character of the thioureide bond. The bond distance of C1–N1 which is at 1.3204(16) Å deviates from the value reported for simple C–N at 1.47 Å,[42] but comparable to the C–N bond found in pyridine. These observations in the CS and CN bond values indicates that the delocalization of the π-electrons occurs throughout the ligand backbone.[43] There are both intramolecular C—H. . . . . S interactions such as C(2)—H(2b). . . S(2), and intermolecular interactions such as C(3)—H(3c). . . S(2i). The intramolecular interactions in the system forms a 4-membered ring involving the thioureide C and N atoms, the methine C atom and the S atom of the dithiocarbamate molecule, while the combination of the intermolecular and the

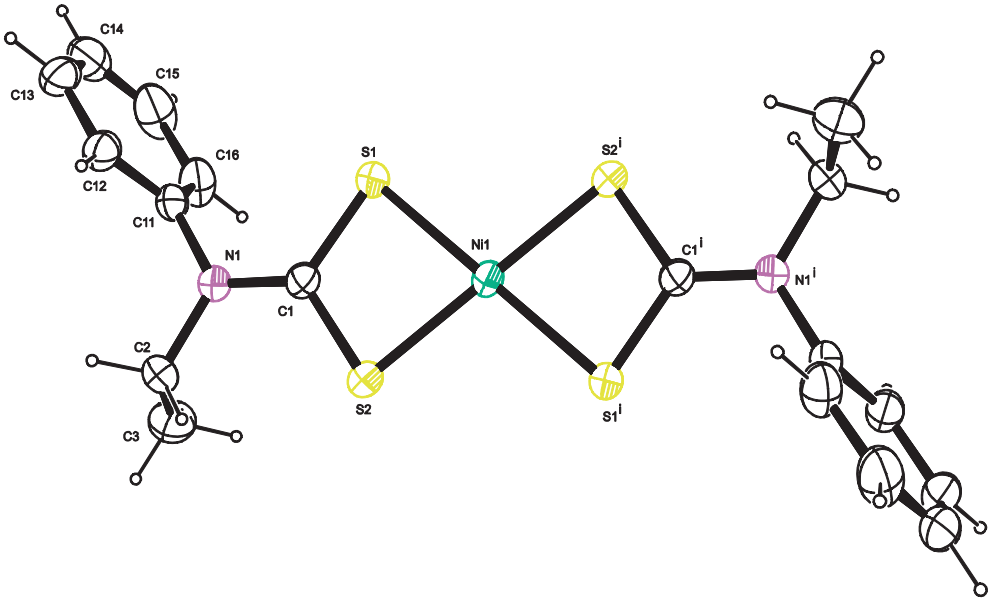

Figure 2. The molecular structure of [NiL$_2^1$] with displacement ellipsoids drawn at 50% probability level.

Table 2. Crystal data, data collection and refinement parameters.

Complex	NiL^1_2	$NiL^1L^2L^3$
Empirical formula	$C_{18}H_{20}N_2NiS_4$	$C_{28}H_{25}N_2NPS_3$
Formula weight	451.29	575.34
Crystal system	monoclinic	monoclinic
Crystal habit	green blocks	red blocks
Space group	P21/n	P21/c
a (Å)	7.4619(3)	16.7079(6)
b (Å)	7.0012(3)	8.1593(3)
c (Å)	19.2781(9)	20.0472(7)
α (°)	90	90
β (°)	93.679(2)	93.770(1)
γ (°)	90	90
U (Å^3)	1005.06(8)	2727.02(17)
Z	2	4
Dcalc (g cm^{-3})	1.491	1.401
μ (MoKa) [/mm]	1.384	1.020
F(000)	468	1192
Crystal size (mm)	0.19 × 0.39 × 0.55	0.04 × 0.31 × 0.33
Temperature (K)	200	200
θ range (°)	2.1–28.3	2.0–28.3
Dataset	−9:9; −9:9; −25:25	−22:22; −10:10; −26:17
Tot., Uniq. Data, R(int)	27461, 2499, 0.016	37614, 6777, 0.022
Observed reflections $I > 2\sigma(I)$	2330	5656
Nref, Npar	2499, 116	6777, 317
R	0.0208	0.0250
w$R2$	0.0544	0.0609
S	1.12	1.03
Max. and Av. shift/error	0.00, 0.00	0.00, 0.00
Min. residual. density. [e/Å∧ 3]	−0.22	−0.28
Max.residual. density. [e/Å∧ 3]	0.26	0.32

Table 3. Selected bond distances and angles for complexes NiL^1_2 and $NiL^1L^2L^3$.

$[NiL^1_2]$		$[NiL^1L^2L^3]$	
Bond	distances (Å)	Bond	distances (Å)
Ni1 – S1	2.2106(4)	Ni1 – S1	2.2282(5)
Ni1 – S2	2.1917(4)	Ni1 – S2	2.1798(5)
Ni1 – S1_a	2.2106(4)	Ni1 – P1	2.1845 (5)
Ni1 – S2_a	2.1917(4)	Ni1 – N2	1.8662(13)
S1 – C1	1.7115(14)	S1 – C1	1.7133(15)
S2 – C1	1.7187(13)	S2 – C1	1.7224(14)
N1 – C1	1.3204(16)	N1 – C1	1.3149(18)
N1 – C2	1.4785(18)	N1 – C2	1.479(2)
N1 – C11	1.4415(17)	N1 – C11	1.4490(19)
Bond	angles (°)	Bond	angles (°)
S1 – Ni1 – S2	7966(1)	S1 – Ni1 – S2	79.14 (2)
S1 – Ni1 – S1_a	180.00	S1 – Ni1 – P1	173.70(2)
S1 – Ni1 – S2_a	100.34(1)	S1 – Ni1 – N2	95.68(4)
Ni1 – S1 – C1	84.54(4)	S2 – Ni1 – P1	95.60(2)
Ni1 – S2 – C1	84.97(5)	P1 – Ni1 – N2	89.84(4)
C1 – N1 – C2	121.76(11)	Ni1 – S1 – C1	84.94(5)
C1 – N1 – C11	121.22(11)	Ni1 – S2 – C1	86.25(5)
C2 – N1 – C11	116.59(10)	C1 – N1 – C2	121.14(12)
S1 – C1 – S2	110.59(7)	C1 – N1 – C11	120.93(12)
		C2 – N1 – C11	117.92(11)
		S1 – C1 – S2	109.64(8)
		S3 – C4 – N2	179.18(14)

Symmetry element a: 1 −x, −y, 1 −z.

intramolecular interactions result in the formation of 6-membered ring, as shown in Figure 3.

Similar to compound $\mathbf{NiL^1_2}$, compound $\mathbf{NiL^1L^2L^3}$ (Figure 4) also crystallizes in monoclinic crystal system, with a space group of $P21/c$. Table 2 contains summary of structure refinement parameters, and selected bond lengths and angles are given in Table 3. The complex has four molecules in the unit cell. The structure

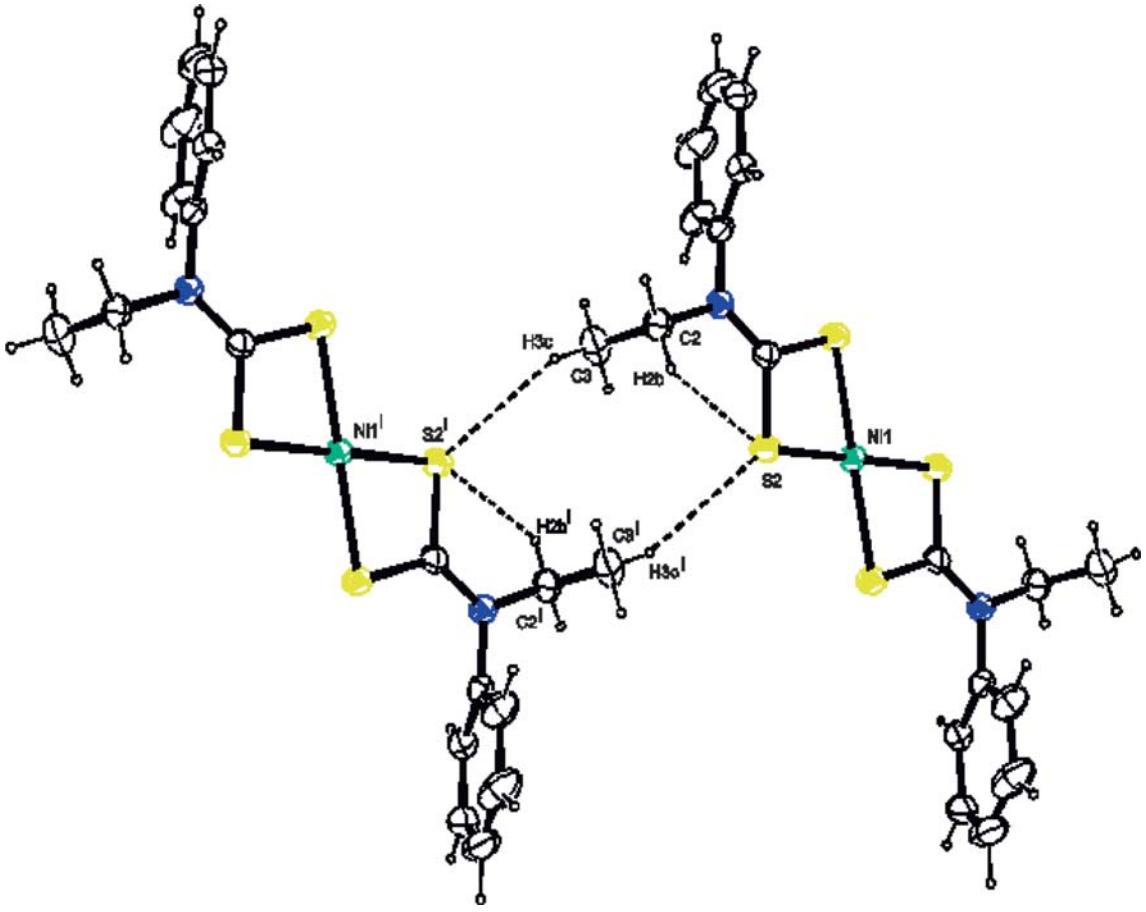

Figure 3. Hydrogen interactions. Symmetry elements: (i) 1-x, -y, 1-z.

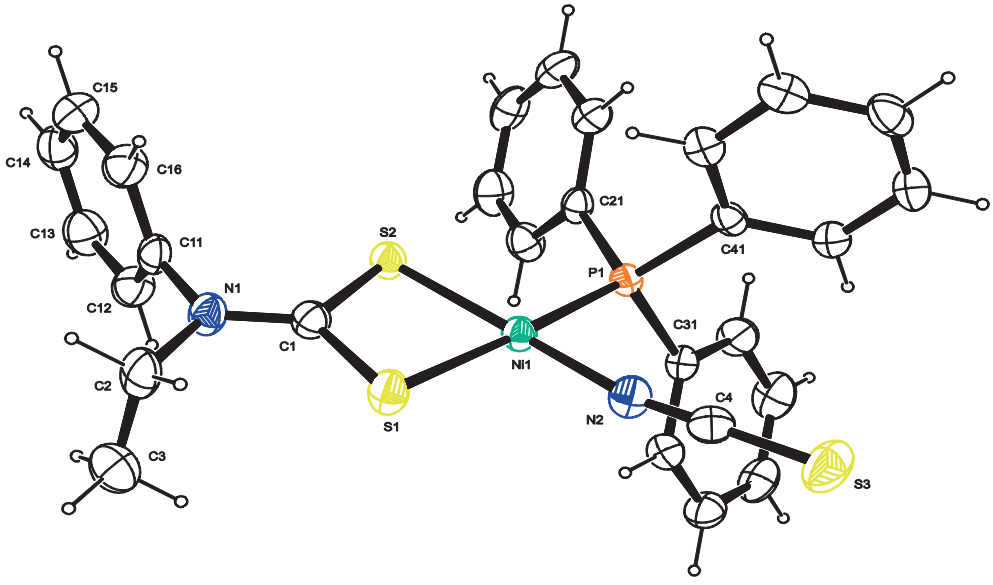

Figure 4. The molecular structure of $[NiL^1L^2L^3]$ with displacement ellipsoids drawn at 50% probability level. C19—O5—C13—C12.

consists of NiS_2PN chromophore generated by a nickel cation coordinated by two sulphur atoms from *N*-ethy-*N*-phenyl dithiocarbamate, one nitrogen atom from the thiocyanate and one phosphorus atom from PPh_3 to form a distorted square planar configuration. There is a more significant deviation from perfect square planar geometry compared to the parent compound NiL_2^1, and this is a result of the inter-ligand coordination angles caused by the small bite angle of the dithiocarbamate ligand [79.14(2)°] and also the steric influence exerted by the bulky PPh_3 ligand. The Ni–S bonds are asymmetric; Ni1–S1 is at 2.2282(5) Å and the Ni1–S2 is at 2.1798(5) Å. The asymmetry has been ascribed to the differences in the trans influence exerted by PPh_3 and NCS. PPh_3 is a good π-acceptor, hence it has greater trans influence than NCS which leads to more elongation of the Ni–S bond *trans* to PPh_3.[33] Similar to $\mathbf{NiL_2^1}$, the backbone of the dithiocarbamato ligand in $\mathbf{NiL^1L^2L^3}$ also show evidence for the delocalization of π-electrons in the C–S and N–C distances. Thioureide C–N distance [1.3149(18) Å] is comparable to other similar compounds.[33,44] The hydrogen bonding and C—H$\cdots\pi$ ring interactions are shown in Figure 5. There is potentially one intramolecular C—H$\cdots$S hydrogen bond involving the hydrogen of the methine carbon [C(2)—H(2B). . .S1] of the ethyl substituent and the S1 atom of the dithiocarbamate molecule. There are a number of intermolecular C—H$\cdots$ ..π ring interactions involving the phenyl rings of the PPh_3 and also the phenyl rings of the dithiocarbamate molecule, such as C(12)—H(12). . . Cg(2), C(14^{i})—H(14^{i}). . . Cg(1), and C(33^{ii})—H(33^{ii}). . . Cg(3). There are no $\pi - \pi$ ring interactions in the system.

3.5 *Comparison of structural parameters between experimental and theoretical data*

It is appropriate here to correlate the structural parameters obtained from the crystal structure studies with computational data. Figure 6 shows the optimized molecular structures for $\mathbf{NiL_2^1}$ and $\mathbf{NiL^1L^2L^3}$. Comparison of the selected bond lengths and bond angles are given in Table 4. The optimized geometry analysis reveals that the molecular geometry is in agreement with the experimental finding. Deviation in the experimental and theoretical bond lengths are less than 0.10 Å for both complexes. The maximum deviation in the bond angles is less than 3° for both complexes. The small discrepancies in bond lengths and bond angles points to the agreement between experimental and theoretical studies. Although theoretical results have

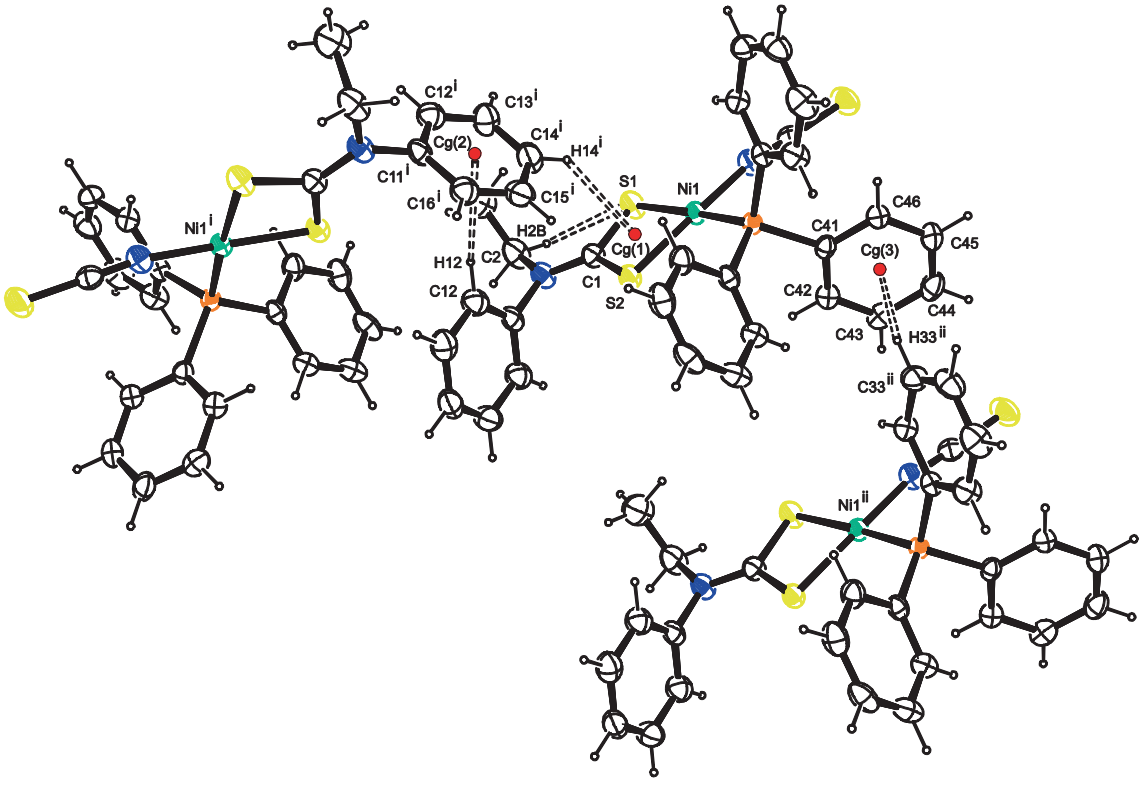

Figure 5. Hydrogen and C—H$\cdots\pi$ ring interactions. Cg(1), Cg(2) and Cg(3) are the centroids of the rings Ni1, S1, C1, S2; C11 – C16; and C41 – C46 respectively. Symmetry elements: (i) 1-x, 1/2+y, 1/2 -z; (ii) x, -1+y, z.

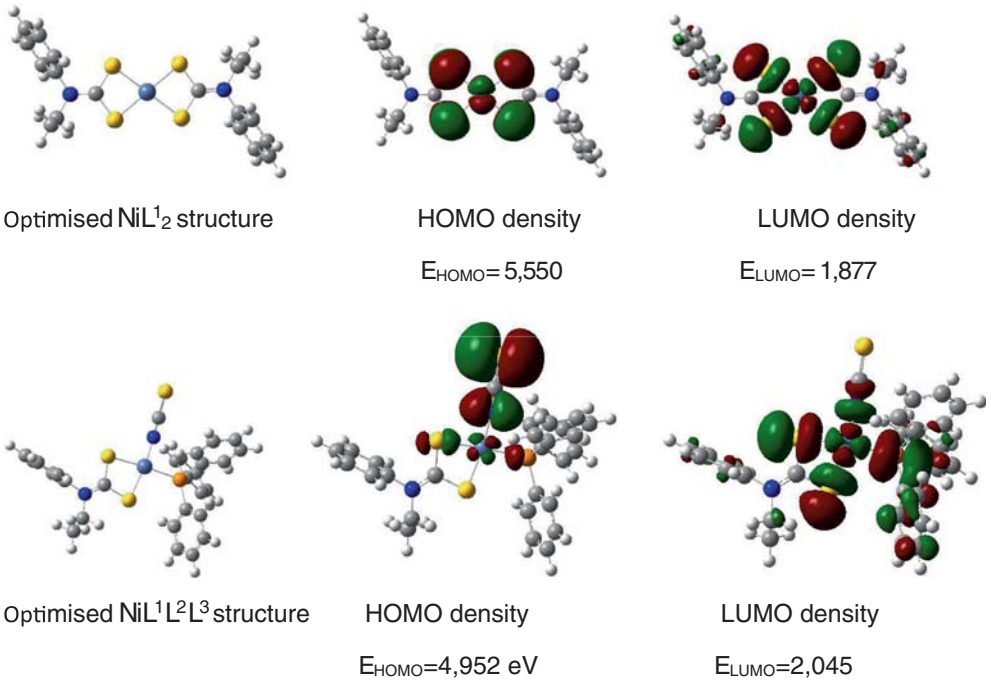

Figure 6. Optimised structure, HOMO and LUMO densities for the studied complexes. The energy of the HOMO and LUMO are shown below each of the structures.

minimal differences from experimental findings, bond lengths from theoretical studies are often larger than the experimental values, due to the fact that theoretical calculations belong to isolated molecule in gaseous phase and the experimental results belong to molecules of the crystal (as a result of crystal packing) in the solid state, where relevant intermolecular interactions play significant role in keeping molecules together.

The crystal structure of $\mathbf{NiL^1L^2L^3}$ shows an evidence of a single intramolecular hydrogen bond corresponding to C2-H2$\cdots$S1, whose H2$\cdots$S1 bond length (Å) is 2.6700, C2$\cdots$S1 bond distance of 3.073 Å and bond angle of 105°. Theoretical studies also predict this intramolecular hydrogen bond with H2$\cdots$S1 bond length (Å) of 2.608, C2$\cdots$S1 bond distance of 3.095 Å and bond angle of 106°. In addition, the theoretical studies show the existence of intramolecular hydrogen bonds involving the C32-H32 of the aromatic ring and N2 atom. The C32–H32$\cdots$N2 bond has the H32$\cdots$N2 bond length of 2.407 Å, C32$\cdots$N2 bond distance of 3.300 Å and bond angle of 139°.

3.6 *HOMO–LUMO analyses*

The frontier orbitals, HOMO and LUMO take part in chemical reactions. Figure 6 also shows the highest occupied molecular orbitals (HOMO) and lowest unoccupied molecular orbital (LUMO) for $\mathbf{NiL^1_2}$ and $\mathbf{NiL^1L^2L^3}$ complexes. The highest occupied molecular orbital (HOMO) is largely localised on the lone pair of electrons of the sulphur atoms and on the Nickel(II) ions in NiL^1_2, whereas the LUMO is completely localized on the Nickel(II) ion, and the orbitals of the sulphur atoms. The HOMO in $\mathbf{NiL^1L^2L^3}$ is localised on the lone pair of electrons on N2 an S3 atoms, whereas the LUMO is largely localized on the S1, S2 and P1 atoms. The energy gap between the highest occupied and the lowest unoccupied molecular orbitals is a critical parameter in determining molecular electrical transport properties because it is a measure of electron conductivity. The energy gaps observed for $\mathbf{NiL^1_2}$ and $\mathbf{NiL^1L^2L^3}$ are 3,67, 2,91 eV respectively.

3.7 *Atom in molecule (AIM) analysis of the Ni$\cdots$Ligand bonding*

The topology of the electron density distribution $\rho(r)$ and its second derivative (Laplacian, $\nabla\rho(r)$) are closely related to bonding strength and bonding type[45–47] respectively. The value of H and its components, G and V, also provide valuable information on the nature of chemical bond.[48–50] The strongest bonds (such as covalent bonds) are characterised by a negative and relatively large value of V (hartree), a positive value of G (hartree) and a negative value of H (hartree). In covalently bonded systems, both interacting atoms are sharing electrons, which are considerably localized in the inter-nuclear region between the atoms of

Table 4. A comparison of the geometric parameters between crystal data and B3LYP/6-311+G(d,p) results *in vacuo*.

NiL^1_2	Experimental data	Theoretical data	$NiL^1L^2L^3$	Experimental data	Theoretical data
Ni-P	2.1845	2.28621	Ni1-S1	2.2106	2.27896
P-C21	1.8239	1.84081	Ni1-S2	2.1917	2.27834
P-C31	1.8188	1.84081	Ni1-S1_a	2.2106	2.27896
P-C41	1.8150	1.83472	Ni1-S2_a	2.1917	2.27834
Ni-N2	1.8662	1.86066	S1-C1	1.7115	1.72260
N2-C4	1.1613	1.18776	S2-C1	1.7187	1.72627
C4-S3	1.6234	1.62095	N1-C1	1.3204	1.34267
Ni-S1	2.2282	2.29634	N1-C2	1.4785	1.47846
Ni-S2	2.1798	2.25685	N1-C11	1.4415	1.44275
C1-S1	1.7133	1.71838	C2-C3	1.508	1.52819
C1-S2	1.7224	1.73842	C11-C12	1.3829	1.39444
C1-N1	1.3149	1.34112	C11-C16	1.381	1.39422
N1-C2	1.479	1.47948	C12-C13	1.391	1.39269
C2-C3	1.510	1.52934	C13-C14	1.378	1.39419
N1-C11	1.4490	1.44461	C14-C15	1.374	1.39376
S1-Ni1-S2	79.14	77.981	S1-Ni1-S2	79.66	78.15510
S1-Ni1-P1	173.70	175.79652	S1-Ni1-S1_a	180.00	179.99347
S1-Ni1-N2	95.68	94.04577	S1-Ni1-S2_a	100.34	101.83727
S2-Ni1-P1	95.60	97.86679	S1_a-Ni1-S2	100.34	101.85113
S2-Ni1-N2	173.08	172.02081	S2-Ni1-S2_a	180.00	179.99129
P1-Ni1-N2	89.84	90.10934	S1_a-Ni1-S2_a	79.66	78.15649
Ni1-S1-C1	84.94	84.64432	Ni1-S1-C1	84.54	84.54833
Ni1-S2-C1	86.25	85.42340	Ni1-S2-C1	84.97	84.48640
Ni1-P1-C21	117.61	115.97952	C1-N1-C2	121.76	121.94845
Ni1-P1-C31	114.36	112.63514	C1-N1-C11	121.22	120.87251
Ni1-P1-C41	109.09	111.74799	C2-N1-C11	116.59	117.15960
C1-N1-C2	121.14	122.18618	S1-C1-S2	110.59	112.80935
C1-N1-C11	120.93	120.74992	S1-C1-N1	125.00	123.53584
C2-N1-C11	117.92	117.00915	S2-C1-N1	124.42	123.65201
Ni1-N2-C4	169.08	170.70174	N1-C2-C3	111.36	113.14428
S1-C1-S2	109.64	111.95046	N1-C11-C12	119.14	119.32761
S1-C1-N1	125.32	124.53077	N1-C11-C16	119.33	120.22716
S2-C1-N1	125.03	123.51603	C12-C11-C16	121.45	120.41340
N1-C2-C3	111.56	112.72387	C11-C12-C13	118.64	119.71867
S3-C4-N2	179.18	178.75636	C12-C13-C14	120.36	120.10038
S2-Ni1-S1-C1	1.10	−0.17241	S2-Ni1-S1-C1	−3.23	0.18342
N2-Ni1-S1-C1	176.48	−179.8578	S2_a-Ni1-S1-C1	176.77	−179.82090
P1-Ni1-S2-C1	175.41	−179.1643	Ni1-S1-C1-S2	4.33	−0.25702
S2-Ni1-P1-C21	0.00	−9.43423	Ni1-S1-C1-N1	−175.65	−179.66748
S2-Ni1-P1-C31	−119.34	−129.5689	C2-N1-C1-S2	−2.92	−0.07487
S2-Ni1-P1-C41	120.75	110.43203	C11-N1-C1-S1	4.89	−2.37695
Ni1-S1-C1-S2	−1.46	0.23603	C1-N1-C2-C3	−91.10	94.64827
Ni1-S1-C1-N1	177.59	179.65003	C1-N1-C11-C16	74.46	−78.91073

interest. The potential energy density estimated at the BCP has a large value because the electrons are relatively stable in the inter-nuclear region. Strong interactions (also known as shared interactions) are further characterised by negative values of $\nabla^2\rho$. Weak interactions (such as hydrogen bonding) are characterised by closed shell interactions. In this type of bonding, H has positive value and is close to zero, G has positive value and V has negative value. However, the positive value of G predominates over the negative value of V, since the electrons are energetically less stable in the region between two closed-shell systems. Weak interactions (also known as closed-shell interactions) are further characterised by a positive value of $\nabla^2\rho$. The inter-nuclear region is characterised by the depletion of electron density. The metal-ligand interaction has characteristics that represent the mix of shared interactions (strong bonds) and closed-shell interactions (weak bonds). In such systems, the value of H is usually negative and close to zero, as found for strong interactions, but with a positive value of $\nabla^2\rho$, which is a characteristic of weak interactions.[50,51] Another parameter that is utilised in the characterisation of the bonding is the |V|/G ratio; |V|/G $<$ 1 represent closed-shell (ionic)

interactions; $|V|/G > 2$ represent shared (covalent type) interactions; $1 < |V|/G < 2$ represent interactions of intermediate character.[45]

The bond critical point data for $\mathbf{NiL_2^1}$ and $\mathbf{NiL^1L^2L^3}$ complexes are presented in Table 5, for the results *in vacuo*. Among the different types of bonds in $\mathbf{NiL^1L^2L^3}$, the N2-C4 bond has the largest value of ρ followed by the C1-N1 bond. The Ni−Ligand bonds have the lowest values of ρ. Among the Ni−Ligand bonds, Ni-N2 has the highest value of ρ whereas Ni-S2 has the lowest value of ρ. A comparison of the $\nabla^2\rho$ values suggest that P-C bond types (P–C21, P–C31 and P–C41), C1–S1, C1–S2 and all C–N bond types (N1–C2, N1–C11 and N2–C4) have negative values of $\nabla^2\rho$, which suggest that they are shared type of bonding. C4–S3 and all the Ni-Ligand type of bonds (Ni–N2, Ni–P, Ni–S1 and Ni–S2) have negative values of $\nabla^2\rho$, which suggest that they are weak type of interactions. With all type of bonds, V has negative value, G has positive value and H (with the exception of the N2–C4) has negative value. This implies that despite the positive value of $\nabla^2\rho$ for the Ni$\cdots$Ligand bonds, the bonding involved in such interactions is more inclined towards shared interactions than closed shell type of interactions. The values of the |V|/G ratio show that it is >2 for C1–S1, C1–S2, C1–N1, N1–C2, N1–C11, and all the P-C type of bonds (P–C21, P–C31 and P–C41). Taken together with their respective $\nabla^2\rho$ and H values, it is reasonable to infer that these bonds are covalent in nature.

The value of the |V|/G ratio for the Ni$\cdots$ligand interactions lie in the range $1 < |V|/G < 2$ which suggests that these interactions are intermediary between covalent and ionic interactions. However, an individual analysis of the |V|/G ratio, for each bond, suggests that Ni–P, Ni–S1 and Ni–S2 are closer to covalent character than ionic character and Ni–N2 is closer to ionic character than covalent character. This analysis is in agreement with the analysis of the $\nabla^2\rho$ values which shows that the Ni–N2 bond has the highest $\nabla^2\rho$ value, which indicates weak interaction. The N2–C4 bond which shows a positive value of H (indicating weak interactions) has the smallest ratio of |V|/G with a value 0.204. The small value of |V|/G, the positive value of both $\nabla^2\rho$ and H are indicative of the predominantly ionic character nature of the N2–C4 interaction.

Among the different bond types in $\mathbf{NiL_2^1}$, all the Ni–S bonds have ρ value of 0.078 and a positive value of $\nabla^2\rho$, which is a characteristic of weak interactions. Although the values of H for all the Ni–S bonds are

Table 5. Bond critical point data for the ligand$\cdots$Fe^{n+} complexes, B3LYP/6-31+G(d,p) results *in vacuo*.

Complex and bond parameter	ρ (Hartree)	$\nabla^2\rho$ (Hartree)	V (Hartree)	G (Hartree)	H (Hartree)	$\frac{\lvert V\rvert}{G}$
$NiL^1L^2L^3$						
Ni-P	0.084	0.808	−0.1022	0.0612	−0.0410	1.670
P-C21	0.160	−0.132	−0.2779	0.1225	−0.1554	2.269
P-C31	0.161	−0.156	−0.2755	0.1183	−0.1572	2.329
P-C41	0.162	−0.149	−0.2816	0.1221	−0.1595	2.306
Ni-N2	0.113	0.556	−0.2022	0.1706	−0.0316	1.185
N2-C4	0.432	−0.110	−0.1505	0.7387	0.5882	0.204
C4-S3	0.216	0.240	−0.5571	0.3085	−0.2486	1.806
Ni-S1	0.083	0.122	−0.1058	0.0681	−0.0377	1.553
Ni-S2	0.077	0.099	−0.9437	0.0595	−0.8842	15.86
C1-S1	0.203	−0.405	−0.2867	0.0927	−0.194	3.094
C1-S2	0.208	−0.375	−0.3625	0.1344	−0.2281	2.698
C1-N1	0.333	−0.895	−0.8584	0.3173	−0.5411	2.706
N1-C2	0.249	−0.659	−0.4293	0.1323	−0.297	3.244
N1-C11	0.271	−0.804	−0.4955	0.1472	−0.3483	3.365
NiL_2^1						
Ni1-S1	0.078	0.167	−0.0869	0.0644	−0.0226	1.351
Ni1-S2	0.078	0.165	−0.0868	0.0640	−0.0228	1.357
Ni1-S1_a	0.078	0.167	−0.0870	0.0644	−0.0226	1.351
Ni1-S2_a	0.078	0.165	−0.0868	0.0640	−0.0228	1.357
S1-C1	0.210	−0.413	−0.2947	0.0957	−0.1990	3.078
S2-C1	0.211	−0.418	−0.3032	0.0994	−0.2038	3.050
N1-C1	0.337	−1.046	−0.7300	0.2342	−0.4957	3.116
N1-C2	0.250	−0.625	−0.3957	0.1198	−0.2760	3.305
N1-C11	0.276	−0.786	−0.4530	0.1282	−0.3248	3.533

negative, they are close to zero, indicating that they have minimal covalent character. The |V|/G ratio for the Ni-S bonds have values in the lower range of the $1 < |V|/G < 2$ range, which suggests that the Ni-S bonds are largely ionic in character than covalent in nature. All the S–C and N–C bond have large values of ρ, with the values of ρ having a range of S–C $< \rho <$ N–C. This range suggests that N–C bond are stronger than S–C bonds. The $\nabla^2\rho$ values are all negative, which indicates strong interactions. Considering that the value of H is also largely negative and the ratio $|V|/G > 2$, it is reasonable to infer that all the S–C and N–C bonds are predominantly covalent in character.

4. Conclusion

This work reports the preparation and characterization of two nickel(II) dithiocarbamates of the composition $[NiL^1_2]$ and $[NiL^1L^2L^3]$ (L^1 = *N*-ethyl-*N*-phenyldithiocarbamato anion, L^2 = isothiocyanato anion, and L^3 = triphenylphosphine). Spectral and structural characterization of the compounds were carried out and analysed. Thermal analysis of the compounds indicated the formation of NiS as end product at the end of the decomposition process. The X-ray structural studies of the complexes showed that the homoleptic $[NiL^1_2]$ complex is centrosymmetric and a monomer with a distorted square-planar geometry, while the heteroleptic $[NiL^1L^2L^3]$ is a non-centrosymmetric monomer with a more distorted square planar geometry. The experimental structural parameters of the complexes were compared with theoretically generated data. The geometric parameters obtained from DFT/B3LYP calculations correlate well with the experimentally observed X-ray crystallographic data. The structure of $NiL^1L^2L^3$ is supported by a weak intermolecular C–H$\cdots$S interactions and gives support to molecular packing stability in the unit.

Supplementary Information (SI)

Crystallographic data of the complexes have been deposited with the Cambridge Crystallographic Data Center allocated with the deposit number CCDC1436866, and CCDC 1406200. Copy of the data can be obtained free of charge on application to CCDC, 12 Union Road, Cambridge CB2 1EZ, UK, fax: +44 1223 336033, email:deposit@ccdc.cam.ac.uk.

References

1. Pastorek R, Štarha P, Drahoš B and Trávníček Z 2014 *Polyhedron* **69** 174
2. Bajia S C and Mishra A 2011 *J. Coord. Chem.* **64** 2727
3. Sigel A, Sigel H and Sigel R K O 2007 In *Nickel and Its Surprising Impact in Nature: Metal Ions in Life Sciences* (Chichester, UK: John Wiley)
4. Trávníček Z, Pastorek R and Slovák V 2008 *Polyhedron* **27** 411
5. Burns R P, McCullough F P and McAuliffe C A 1980 *Adv. Inorg. Chem. Radiochem.* **23** 211
6. Geetha N and Thirumaran S 2008 *J. Serb. Chem. Soc.* **73** 169
7. Prakasam B A, Ramalingam K, Bocelli G and Olla R 2004 *Z. Anorg. Allg. Chem.* **630** 301
8. Galland J-C, Savignac M and Genêt J-P 1999 *Tetrahedron Lett.* **40** 2323
9. Nan Y and Yang Z 1999 *Tetrahedron Lett.* **40** 3321
10. Srogl J, Liu W, Marshall D and Liebeskind L S 1999 *J. Am. Chem. Soc.* **121** 9449
11. Sambaiah T, Li L, Huang D, Lin C, Rayabarapu D K and Cheng C 1999 *J. Org. Chem.* **64** 3663
12. Jan Rabek F 2012 In *Polymer Photodegradation: Mechanisms and experimental methods* (Berlin: Springer Science and Business Media)
13. Hollingsworth N, Roffey A, Islam H-U, Mercy M, Roldan A, Bras W, Wolthers M, Catlow C R A, Sankar G, Hogarth G and de Leeuw N H 2014 *Chem. Mater.* **26** 6281
14. Venkatachalam V, Ramalingam K, Bocelli G and Cantoni A 1997 *Inorg. Chim. Acta* **257** 49
15. Manohar A, Ramalingam K, Thiruneelakandan R, Bocelli G and Righi L 2006 *Z. Anorg. Allg. Chem.* **632** 461
16. Thiruneelakandan R, Ramalingam K, Bocelli G and Righi L 2005 *Z. Anorg. Allg. Chem.* **631** 187
17. Trávníček Z, Pastorek R, Štarha P, Popa I and Slovák V 2010 *Z. Anorg. Allg. Chem.* **636** 1557
18. Prakasam B A, Ramalingam K, Bocelli G and Cantoni A 2006 *Bull. Chem. Soc. Jpn.* **79** 113
19. Srinivasan S, Ramalingam K and Rizzoli C 2012 *Polyhedron* **33** 60
20. Patra A, Mondal B, Sen B, Zangrando E and Chattopadhyay P 2015 *J. Chem. Sci.* **127** 1883
21. Anitha P, Manikandan R, Vijayan P, Prakash G, Viswanathamurthi P and Butcher R J 2015 *J. Chem. Sci.* **127** 597
22. Kumar S C, Pal A, Mitra M, Manikandamathavan V M, Lin C-H, Nair B U and Ghosh R 2015 *J. Chem. Sci.* **127** 1375
23. Shahabadi N and Fatahi A 2010 *J. Mol. Struct.* **970** 90
24. Skyrianou K C, Efthimiadou E K, Psycharis V, Terzis A, Kessissoglou D P and Psomas G 2009 *J. Inorg. Biochem.* **103** 1617
25. Pastorek R, Kameníček J, Cvek B, Pavlíček M, Šindelář Z and Žák Z 2003 *J. Coord. Chem.* **56** 1123
26. APEX2, SADABS and SAINT 2010 Bruker AXS Inc., Madison, Wisconsin, USA
27. Sheldrick G M 2008 *Acta Cryst.* **A64** 112
28. Hübschle C B, Sheldrick G M and Dittrich B 2011 *J. Appl. Cryst.* **44** 1281

29. Gaussian 09, Revision *C.01*, Frisch M J, Trucks G W, Schlegel H B, Scuseria G E, Robb M A, Cheeseman J R, Scalmani G, Barone V, Mennucci B, Petersson G A, Nakatsuji H, Caricato M, Li X, Hratchian H P, Izmaylov A F, Bloino J, Zheng G, Sonnenberg J L, Hada M, Ehara M, Toyota K, Fukuda R, Hasegawa J, Ishida M, Nakajima T, Honda Y, Kitao O, Nakai H, Vreven T, Montgomery J A, Jr., Peralta J E, Ogliaro F, Bearpark M, Heyd J J, Brothers E, Kudin K N, Staroverov V N, Kobayashi R, Normand J, Raghavachari K, Rendell A, Burant J C, Iyengar S S, Tomasi J, Cossi M, Rega N, Millam J M, Klene M, Knox J E, Cross J B, Bakken V, Adamo C, Jaramillo J, Gomperts R, Stratmann R E, Yazyev O, Austin A J, Cammi R, Pomelli C, Ochterski J W, Martin R L, Morokuma K, Zakrzewski V G, Voth G A, Salvador P, Dannenberg J J, Dapprich S, Daniels A D, Farkas O, Foresman J B, Ortiz J V, Cioslowski J, and Fox D J, Gaussian, Inc., Wallingford CT, 2009.
30. Keith T A 2014 AIMAll (Version 14.06.21), TK Gristmill Software, Overland Park KS, USA
31. Onwudiwe D C and Ajibade P A 2010 *Polyhedron* **29** 1431
32. Sathiyaraj E, Srinivasan T, Thirumaran S and Velmurugan D 1102 *J. Mol. Struct.* 203
33. Valarmathi P, Thirumaran S, Sarmal L and Kant R 2014 *Spectrochim. Acta* **129A** 285
34. Fackler J P, Lin I J B and Andrews J 1977 *Inorg. Chem.* **16** 450
35. Rani P J, Thirumaran S and Ciattini S 2013 *Phosphorus, Sulfur, Silicon Relat. Elem.* **188** 778
36. Sovilj S P, Vučković G, Babić K, Sabo T J, Macura S and Juranić N 1997 *J. Coord. Chem.* **41** 19
37. Tiwari A and Raj B 2015 In *Reactions and mechanisms in thermal analysis of advanced materials* (Hoboken, New Jersey: John Wiley)
38. Ondrušová D, Jóna E and Šimon P 2002 *J. Therm. Anal. Calorim.* **67** 147
39. Sharma A K 1986 *Thermochim. Acta* **104** 339
40. Onwudiwe D C, Arfin T and Strydom C A 2014 *Electrochim. Acta* **127** 283
41. Halimehjani A Z, Torabi S, Amani V, Notash B and Saidi M R 2015 *Polyhedron* **102** 643
42. D R Lide (Ed.) 1992 In *Handbook of Chemistry and Physics* 73rd edn. (Boca Raton, FL: CRC Press)
43. Arul P B, Lahtinen M, Peuronen A, Muruganandham M, Kolehmainen E, Haapaniemi E and Sillanpää M 2014 *Polyhedron* **81** 588
44. Trávníček Z, Pastorek R, Štarha P, Popa I and Slovák V 2010 *Z. Anorg. Allg. Chem.* **636** 1557
45. Bader R F W and Matta C F 2001 *Inorg. Chem.* **40** 5603
46. Gervasio G, Bianchi R and Marabello D 2004 *Chem. Phys. Lett.* **387** 481
47. Kabanda M M, Tran V T, Tran T Q and Ebenso E E 2014 *Comp. Theor. Chem.* **1046** 30
48. Feng L, Bai F-Q, Wu Y and Zhang H-X 2011 *Mol. Phys.* **109** 645
49. Kabanda M M 2015 *Eur. Food Res. Technol.* **241** 553
50. Varadwaj P R and Marques H M 2010 *Phys. Chem. Chem. Phys.* **12** 2126
51. Tsiepe T J, Kabanda M M and Serobatse K R N 2015 *Food Biophys.* **10** 342